We are IntechOpen,
the world's leading publisher of
Open Access books
Built by scientists, for scientists

5,300
Open access books available

130,000
International authors and editors

155M
Downloads

154
Countries delivered to

Our authors are among the

TOP 1%
most cited scientists

12.2%
Contributors from top 500 universities

WEB OF SCIENCE™

Selection of our books indexed in the Book Citation Index
in Web of Science™ Core Collection (BKCI)

Interested in publishing with us?
Contact book.department@intechopen.com

Numbers displayed above are based on latest data collected.
For more information visit www.intechopen.com

X-Ray Digital Linear Tomosynthesis Imaging of Arthoroplasty

Tsutomu Gomi[1], Hiroshi Hirano[2] and Masahiro Nakajima[3]
[1]School of Allied Health Sciences, Kitasato University
[2]Department of Radiology, Shinshu University Hospital
[3]Department of Radiology, Dokkyo Medical University Hospital
Japan

1. Introduction

Interest in tomosynthesis and its clinical applications has been revived by recent advances in digital X-ray detector technology. Conventional tomography technology provides planar information of an object from its projection images. In tomography, an X-ray tube and X-ray film receptor are positioned on either side of the object. The relative motion of the tube and film is predetermined based on the location of the in-focus plane (Ziedses des plate 1932). A single image plane is generated by a scan, and multi-slice computed tomography (CT) scans are required to provide a sufficient number of planes to cover the selected structure in the object. Tomosynthesis acquires only one set of discrete X-ray projections that can be used to reconstruct any plane of the object retrospectively (Grant 1972). This technique has been investigated in angiography and imaging of the chest, hand joints, lungs, teeth, and breasts (Stiel et al 1993 , Duryea et al 2003 , Sone et al 1995 , Niklason et al 1997 , Dobbins et al 2003).

2. Performance of tomosynthesis

2.1 General tomosynthesis reconstruction methods

Existing tomosynthesis algorithms can be divided into three categories: (1) backprojection algorithms, (2) filtered backprojection (FBP) algorithms, and (3) iterative algorithms. The Fig.1 view shown here highlights the difficulty in visualizing three-dimensional (3D) information in X-ray radiography. In the Fig.2 view it turns an acquisition direction to avoid superimposition of an object. The three resulting projection images may be shifted and added (SAA) so as to bring either the circles or triangles to coincide (i.e., focus), with the complementary object smeared out. The basis for FBP is the backprojection of data acquired in projections acquired over all angles. This procedure is performed for each pixel in a projection, and for all possible angles of the projected data, then one has created a simple backprojection image of the object (Fig.3). The backprojection algorithm is referred to as "SAA", whereby projection images taken at different angles are electronically SAA to generate an image plane focused at a certain depth below the surface. The projection shift is adjusted so that the visibility of features in the selected plane is enhanced while that in other planes is blurred. Using a digital detector, image planes at all depths can be retrospectively

reconstructed from one set of projections. The SAA algorithm is valid only if the motion of the X-ray focal spot is parallel to the detector.
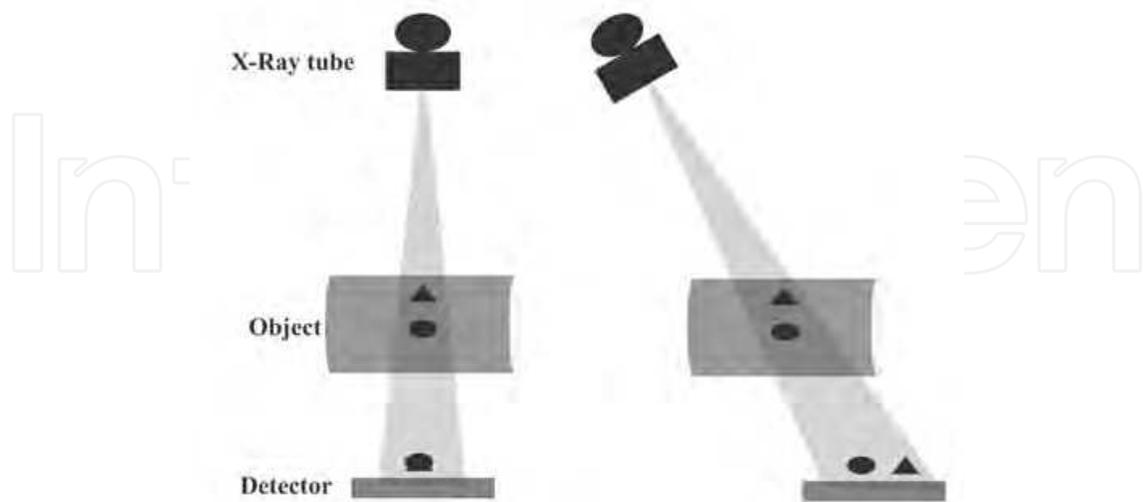

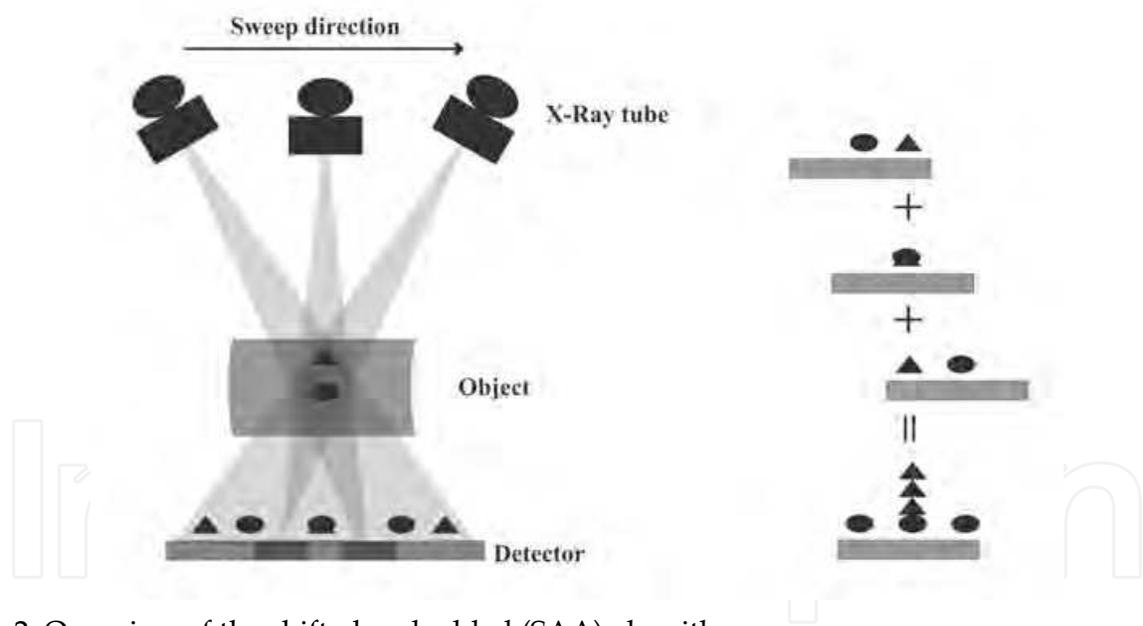Fig. 1. Overview of the conventional radiography method.

Fig. 2. Overview of the shifted and added (SAA) algorithm.

FBP algorithms are widely used in CT in which many projections acquired at greater than 360 degrees are used to reconstruct cross-sectional images. The number of projections typically ranges between a few hundred to about one thousand. The Fourier central slice theorem is fundamental to the FBP theory. In two-dimensional (2D) CT imaging, a projection of an object corresponds to sampling the object along the direction perpendicular to the X-ray beam in the Fourier space (Kak et al 1988). For many projections, information about the object is well sampled and the object can be restored by combining the information from all projections. In 3D cone-beam imaging, the information about the
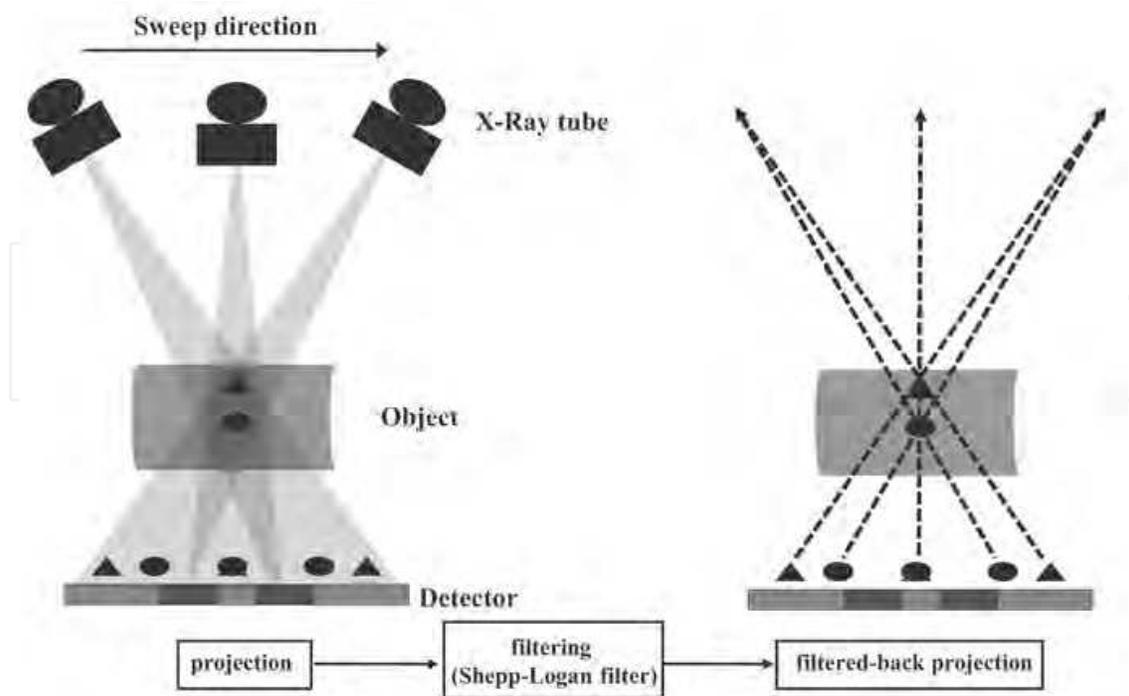
Fig. 3. Overview of the filtered backprojection (FBP) algorithm.

object in Fourier space is related to the Radon transform of the object. The relationship between the Radon transform and cone-beam projections has been well studied and solutions to the cone-beam reconstruction have been provided (Smith 1985).The FBP algorithm generally provides a high degree of precision for 3D reconstruction images when an exact type algorithm is employed (Feldkamp et al 1984) (see Appendix). Therefore, this method has been adopted for image reconstruction of 3D tomography and multi-detector cone-beam CT.

An iterative algorithm performs the reconstruction in a recursive fashion (Ruttimann et al 1984 , Bleuet et al 2002), unlike the one-step operation in backprojection and FBP algorithms. During iterative reconstruction, a 3D object model is repeatedly updated until the model converges to the solution that optimizes an objective function. The objective function defines the criteria of the reconstruction solution. The objective function in the maximum likelihood (ML) algorithm is the likelihood function, which is the probability of getting the measured projections in a given object model. The solution of the ML algorithm is an object model that maximizes the probability of getting the measured projections.

2.2 Radiography vs. tomosynthesis

Anteroposterior (AP) radiograph of these joints demonstrate the excellent visualization of the prostheses in this view. AP radiograph is difficult to visualize 3D information in an AP radiograph as shown (Fig.4). An alternative approach to tomosynthesis imaging is to determine the number of views that can be acquired given imaging constraints (e.g., time restrictions from patient motion, dose restrictions of the detector). The tomographic angle can be selected to yield images with an acceptable level of artifacts. This is certainly the case with FBP algorithm and is suspected to be the case with simple backprojection (or the SAA algorithm). It is possible, however, that this restriction could be reduced by the use of an alternative reconstruction scheme.

2.3 CT vs. tomosynthesis

Imaging by X-ray CT has improved over the last three decades and is now a powerful tool in medical diagnostics. CT imaging has become an essential noninvasive imaging technique since the advent of spiral CT imaging in the 1990s, which led to shorter scan times and improved 3D spatial resolution. CT provides high resolution in the tomographic plane but limited resolution in the axial direction. However, the quality of images generated by a CT scanner can still be reduced due to the presence of metal objects in the field of view. Imaging of patients with metal implants, such as marker pins, dental fillings, or hip prostheses, is susceptible to artifacts generally in the form of bright and dark streaks, cupping and capping, etc. This artifact susceptibility is mostly due to quantum noise, scattered radiation, and beam hardening (Hsieh 1995). Metal artifacts influence image quality by reducing contrast and by obscuring details, thus impairing the ability to detect structures of interest and possibly leading to misdiagnosis. In addition, CT values are impaired, which can lead to errors when using these data e.g., for attenuation correction in positron emission tomography (PET)/CT imaging (Kamel et al 2003). The metallic components of arthroplasty devices are high-contrast objects that generate artifacts when imaged using CT scans. These artifacts can make it extremely difficult or impossible to interpret images obtained by devices. The presence of artifacts along with partial volume effect (PVE) severely limits the potential for objective quantification of total joint replacement with CT.
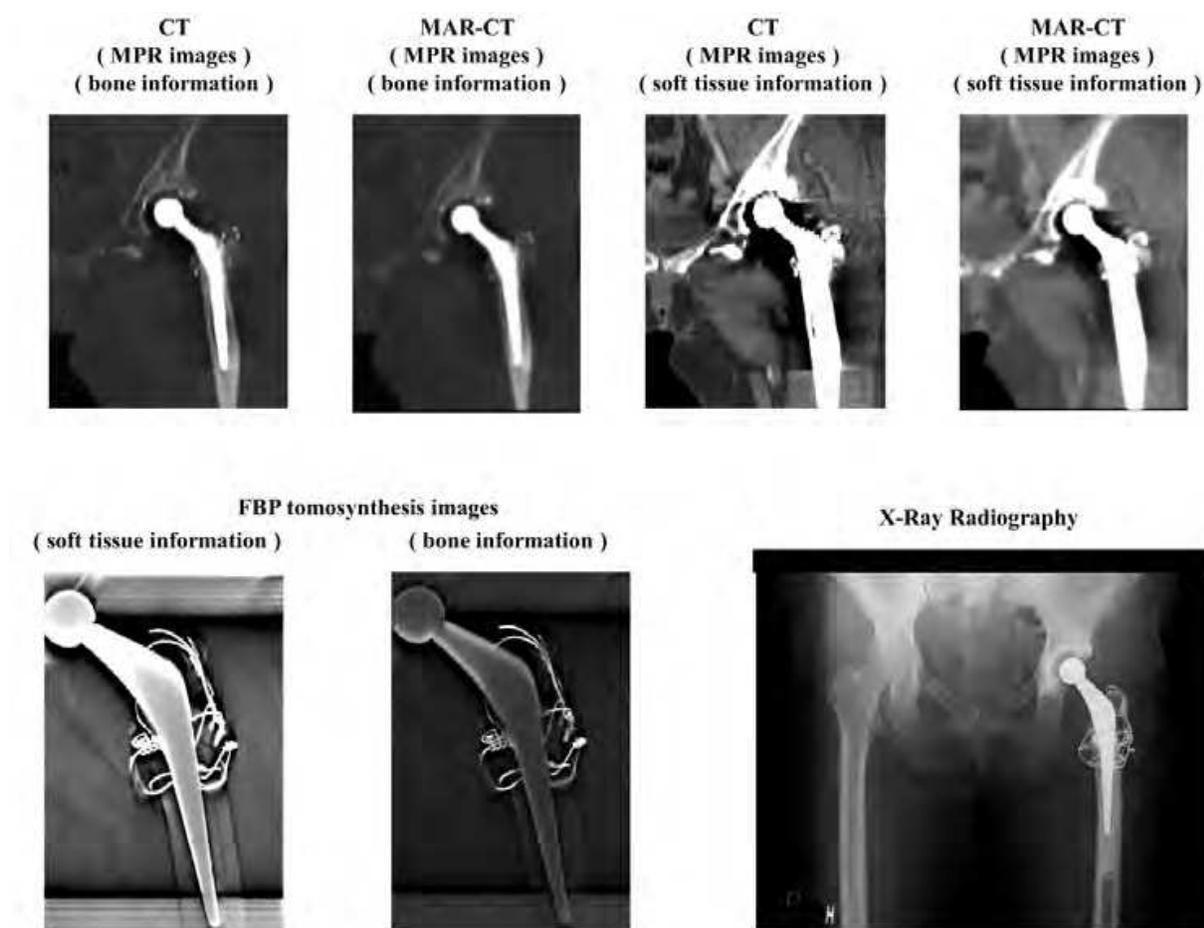
Fig. 4. Patient (52-year-old woman; total hip arthroplasty; THA). Anteroposterior (AP) radiographs of the hip joint prostheses are demonstrated.

Methods for reduction of metal artifacts aim to improve the quality of images affected by these artifacts. In recent years, modified iterative (Wang et al 1996 , 1999 , 2000 , Man et al 2000) or wavelet reconstruction techniques have produced promising results. However, these methods cannot be combined with the fast and robust FBP algorithm, which is the standard reconstruction technique (Robertson et al 1997) implemented in modern CT scanners.

Digital linear tomosynthesis using the FBP algorithm shows adequate overall performance, but its effectiveness depends strongly on the region of the image. Digital linear tomosynthesis using FBP algorithm images gives good results independent of the type of metal present in the patient and shows good results for the removal of noise artifacts, especially at greater distances from metal objects. Application of digital linear tomosynthesis to the imaging of hip prostheses appears promising. In addition, flexibility in the choice of digital linear tomosynthesis imaging parameters based on the desired final images and generation of high quality images may be beneficial.

In Fig.4, Coronal slice images (multi-planar reconstruction; MPR) of the hip prosthesis at center heights on metal artifact reduction (MAR) CT (MAR-CT) and non MAR-CT scans at approximately the same level. Remarkable metal artifacts can be seen occurring in the neighborhood of the hip prosthesis. However, MAR-CT processing reduced the metal artifacts. Tomosynthesis images of the prostheses at center heights at the same level. The new diagnostic information that could not be acquired from CT images is provided. Reduction in metal artifacts was obtained in the images as shown here. The use of tomosynthesis allowed better visualization of the prosthesis caused by the blurring of anatomic structures above and below the visualized planes.

The FBP tomosynthesis was compared to MAR CT, and non-MAR CT scans of a prosthesis case. The effectiveness of this method in enhancing visibility of a prosthesis case was quantified in terms of the signal-to-noise ratio (SNR), and removal of ghosting artifacts in a prosthesis case was quantified in terms of the artifact spread function (ASF). The SNR in the prosthetic case was determined. The SNR is defined as $\frac{N_1 - N_0}{\sigma_0}$, where N_1 is the mean pixel value in the region of interest (ROI) within the object, N_0 is the mean pixel value in the ROI in a background area, and σ_0 is the standard deviation of pixel values in the background ROI. Throughout these results, σ_0 includes structure noise that can obscure the object, in addition to photon statistics and electronic noise. Wu et al. proposed an ASF metric to quantify artifacts observed in planes outside the focus image plane (Wu et al 2003). The artifacts are generated from real features located in the focus image plane, and resemble the real feature. The artifacts exhibited in image planes are defined by the ASF as $\frac{N_{artifact}(z) - N_{BG}(z)}{N_{artifact}(z_0) - N_{BG}(z_0)}$, where z_0 is the location of the in-focus plane of the real feature, z is the location of the off-focus plane, and $N_{artifact}$ (z_0) and N_{BG} (z_0) are the average pixel intensities of the feature and the image background in the in-focus plane, respectively, $N_{artifact}(z)$ and N_{BG} (z) are the average pixel intensities of the artifact and the image background in the off-focus plane, respectively.

The effectiveness of this method in enhancing visibility of a prosthesis case was quantified in terms of the SNR, and removal of ghosting artifacts in a prosthesis case was quantified in terms of the ASF. In the near in-focus plane, the contrast is greater in the MAR CT or FBP tomosynthesis relative to the non-MAR CT (Fig.5).
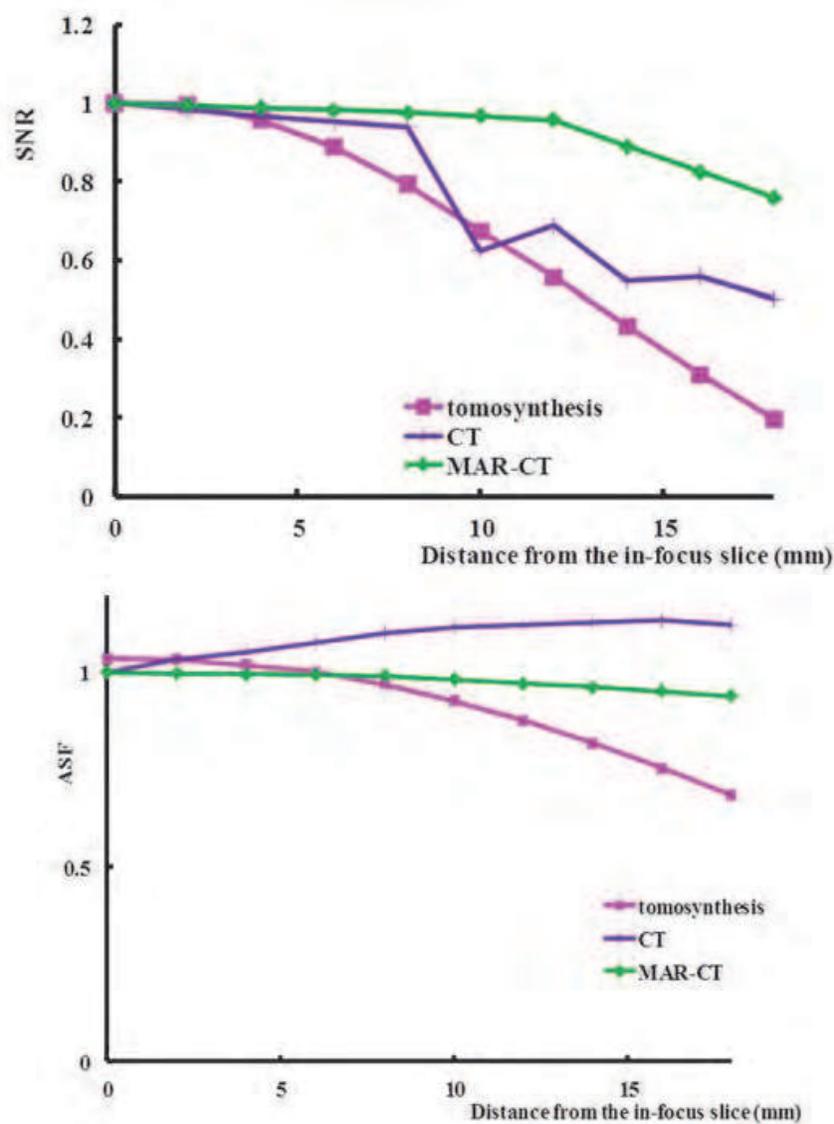
Fig. 5. Metal artefact reduction computed tomography (MAR-CT) with in-focus plane is best for signal-to-noise ratio (SNR) optimization, whereas MAR-CT with off-focus plane is best for SNR optimization. It seems that number of the projection, total exposure dose, and pixel size of detector in MAR-CT gives better results than FBP tomosynthesis. Artifact spread function (ASF) chart demonstrates that FBP tomosynthesis results in maximum removal of metal artifacts.

2.4 Evaluation of artifact reduction for prosthesis imaging

Metal artifacts influence image quality by reducing contrast and obscuring detail, thus impairing the ability to detect structures of interest and making diagnosis impossible. The objective of this report is to evaluate the clinical application of digital linear tomosynthesis in imaging a phantom and hip prosthesis using a relatively new tomosynthesis instrument and applying a selection of reconstruction algorithms. Tomosynthesis images were compared with the results from artifact reduction processing and a FBP algorithm.

Artifacts caused by high-attenuation features in hip prostheses were observed in digital linear tomosynthesis reconstruction as a result of the small number of projections and

narrow angular range typically employed in tomosynthesis imaging. Gomi et al. (Gomi et al 2008 , 2009) developed artifact reduction methods based on a modified Shepp–Logan reconstruction filter kernel by taking into account the additional weight of direct current components in the frequency domain space. Processing leads to an increase in the ratio of low frequency components in an image (see appendix). Artifact reduction processing was performed with a basic and FBP algorithm. Artifact reduction processing provides a method of filtering that can be used in combination with the backprojection algorithm to yield sliced images with desired properties by means of tomosynthesis.
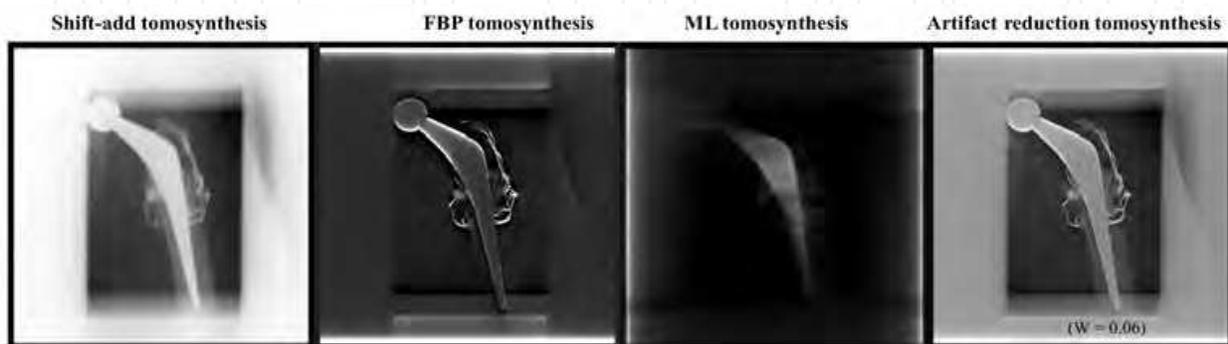

Fig. 6. Comparison of images obtained from artifact reduction tomosynthesis (W= 0.06), FBP tomosynthesis, SAA tomosynthesis, and maximum likelihood tomosynthesis (ML, four subsets & 15 iterations) of the center plane. Artifact reduction tomosynthesis provided better visualization of the hip prosthesis by eliminating blurring and reducing artifacts above and below visualized planes.

The quality of CT images is governed by the strength of artifacts, which depends on numerous factors such as size, shape, density, atomic number and position of metal objects, patient size, and patient's cross-section shape. For small implants manufactured from relatively light metals (e.g., titanium), the effects of beam-hardening and scattering are low. Therefore, the corrupted CT values as well as noise-induced streaking artifacts that pose a major problem to image quality can be neglected. In such cases, the digital linear tomosynthesis approach to artifact reduction processing appears to be promising for the reduction of artifacts stemming from metals with a relatively high atomic number (Fig.6). Improvement of an artificial image (part of undershooting) by an artifact reduction processing is accepted (Fig.7). The effectiveness of the artifact reduction processing method in enhancing the visibility of a prosthetic case was quantified in terms of removal of artifacts. The potential of artifact reduction processing for digital linear tomosynthesis in the evaluation of hip prostheseswas demonstrated. Artifact reduction processing tomosynthesis realize that an especially normal bone and adhesion of an artificial bone become observable (Fig.8-9).

2.5 Potential artifacts
Ideally, structures in a given plane of interest should be clearly displayed in the corresponding tomosynthesis reconstruction plane, whereas structures located outside of that plane should not be visible. Essentially, the limited angular range of the tomosynthesis image acquisition geometry dictates that the spatial resolution is limited in the dimension perpendicular to the detector plane. As a result, out-of-plane structures cannot be

completely removed from the reconstruction plane. Out-of-plane structures are present in every reconstruction plane, but most are not visible because the various low-amplitude structures from projections overlap each other in the reconstruction plane, and therefore are blurred. Out-of-plane structures from high-attenuation features cannot be blurred. They appear as multiple replicates of the particular feature in every reconstruction plane except for the one in which the actual high-attenuation feature is located. At one projection angle, these ghosting features are distributed along the line made by the X-ray source and actual feature (Fig.10).
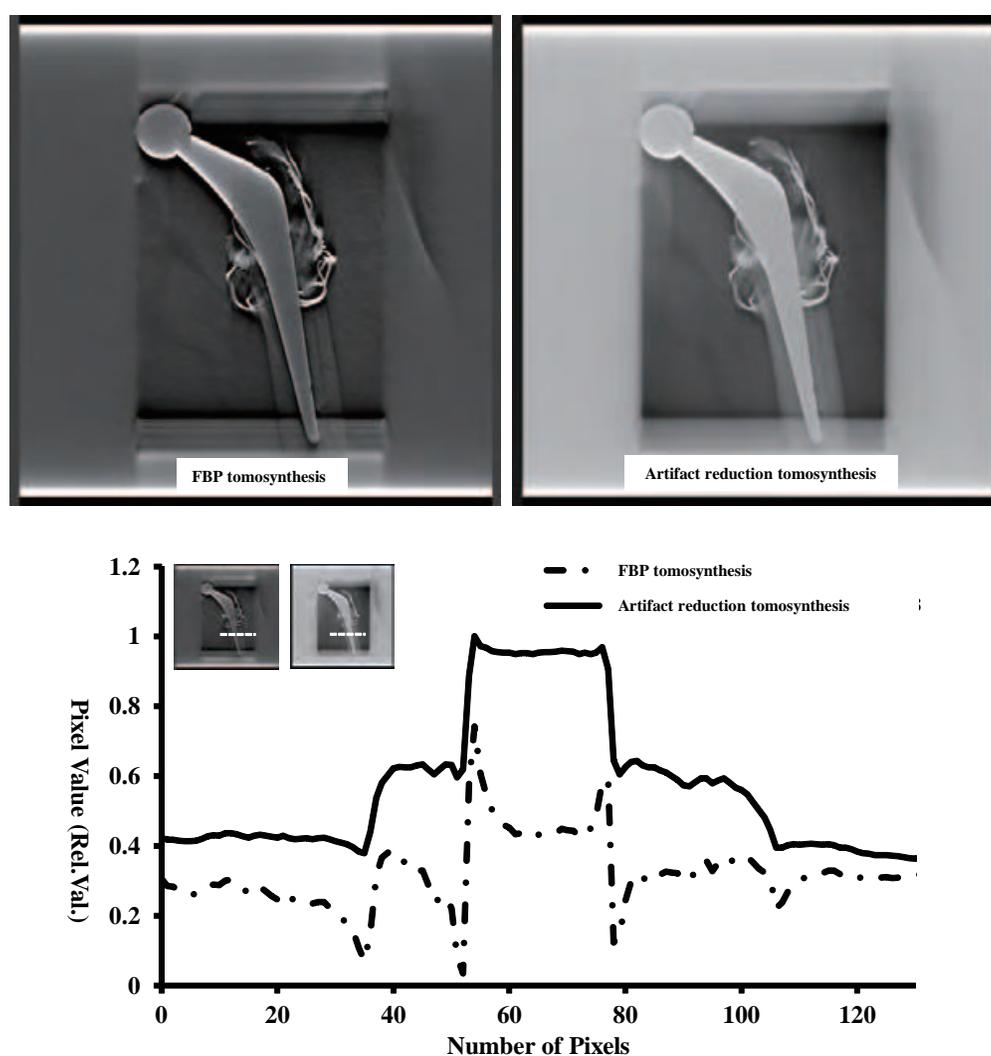

Fig. 7. Comparison of line profiles using artifact reduction processing (W = 0.06) and FBP algorithm in the in-focus plane. Artifacts (part of the undershoot) are reduced by artifact reduction processing.
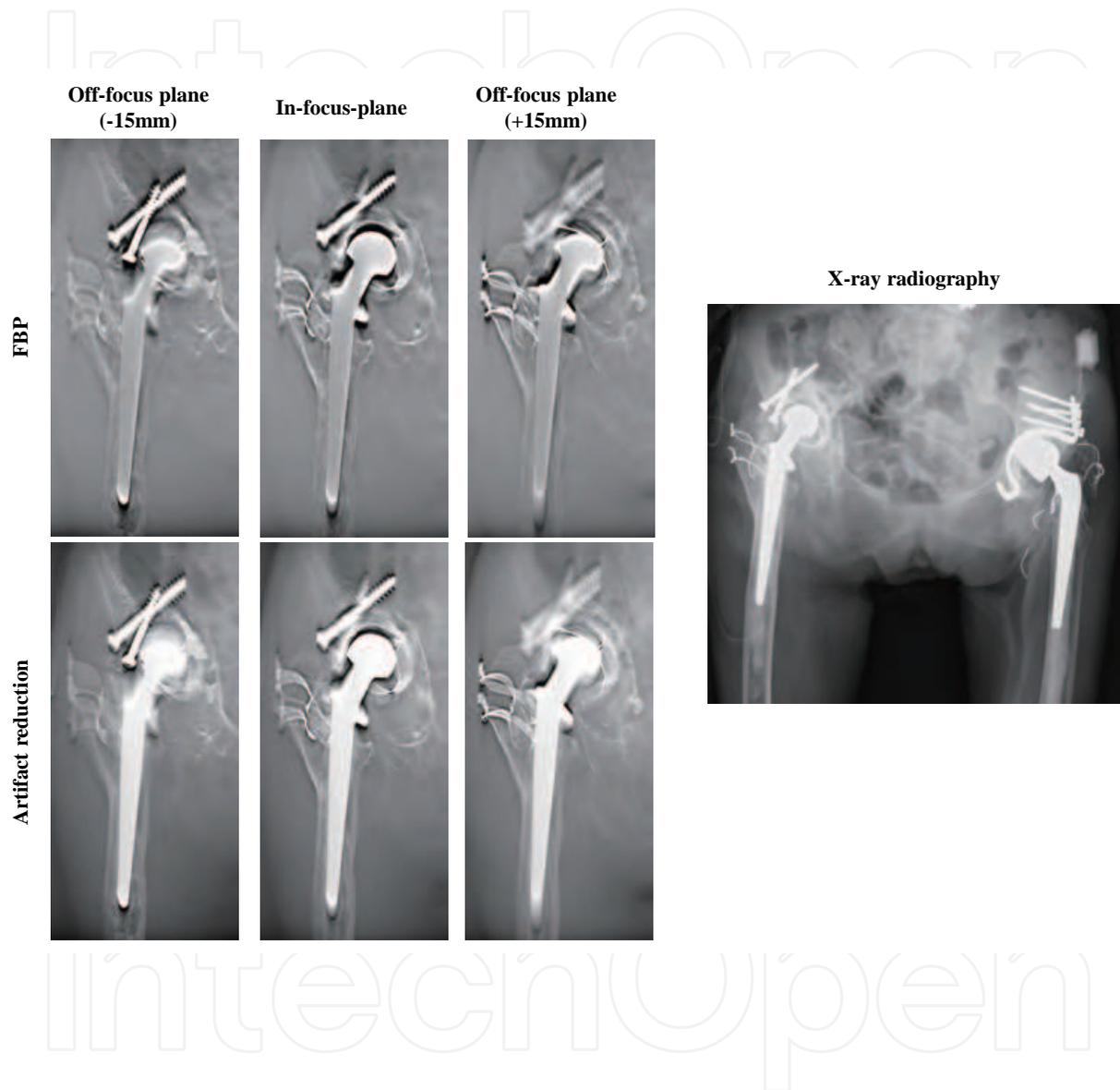
Fig. 8. Case 1 patient (81-year-old woman; Rheumatism, post THA). AP radiographs of the hip joint prostheses are demonstrated. AP radiograph is difficult to visualize 3D information in an AP radiograph as shown. The use of artifact reduction tomosynthesis (w=0.06) allowed better visualization of the right hip joint prosthesis caused by the blurring of anatomic structures above and below the visualized planes.
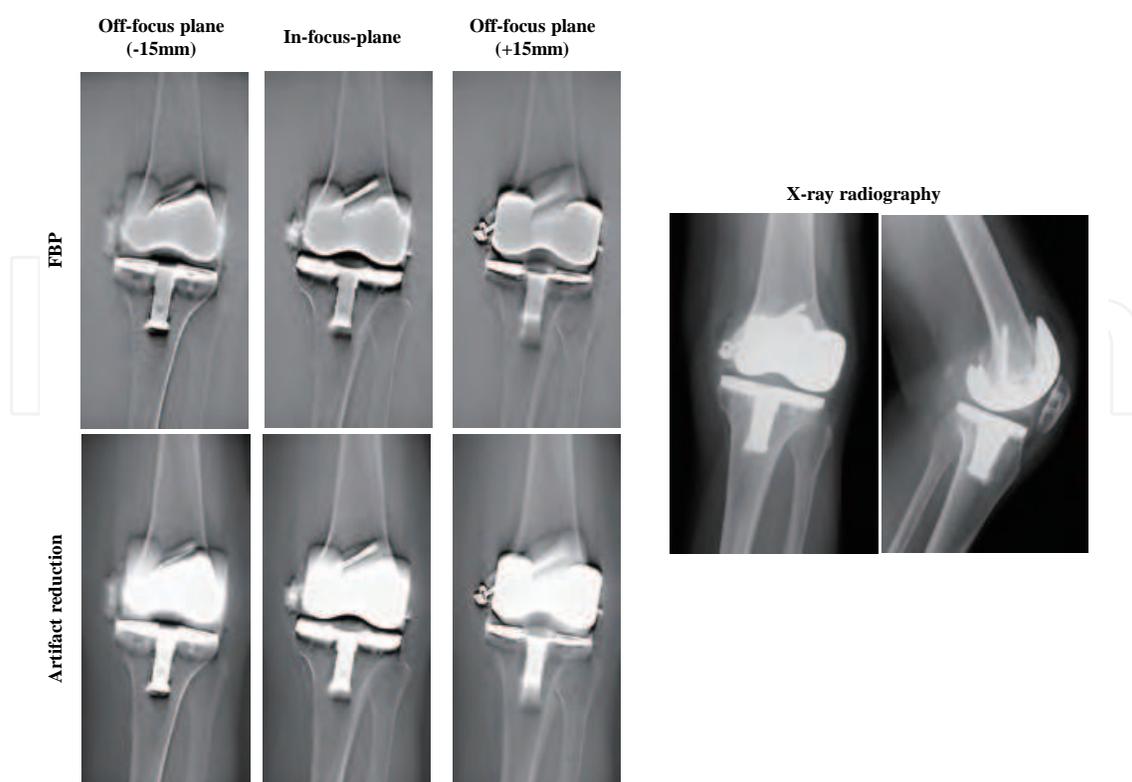
Fig. 9. Case 2 patient (71-year-old woman; Gonarthrosis, post total knee arthroplasty; TKA). AP radiographs of the knee joint prostheses are demonstrated. AP radiograph is difficult to visualize 3D information in an AP radiograph as shown. The use of artifact reduction tomosynthesis (w=0.06) allowed better visualization of the prosthesis caused by the blurring of anatomic structures above and below the visualized planes.
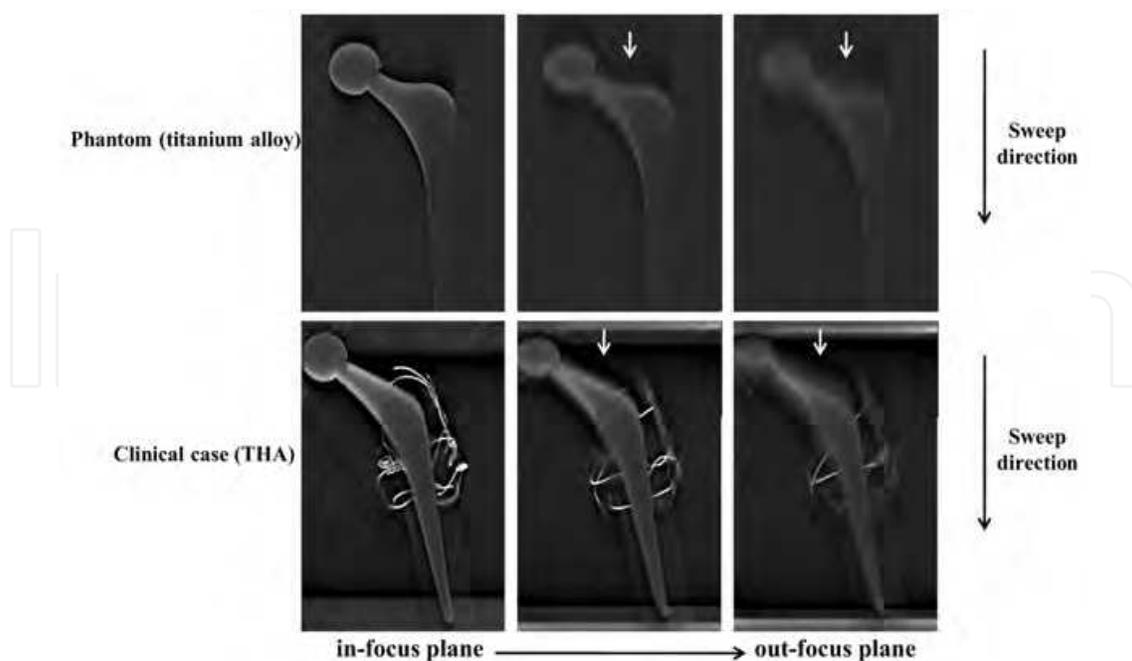

Fig. 10. Blurring occurs along the sweep direction and results from imaging studies show that a high contrast structure exists out of the slice plane that is continuously perpendicular to the sweep direction.

3. Conclusion

The digital linear tomosynthesis images in this review were acquired using linear motion of the X-ray tube and detector. The type of motion used during data acquisition dictates the type of blurring of off-focal-plane objects in the image. Linear motion blurs objects in one dimension only, which leads to linear streak artifacts caused by high-contrast off-focal-plane objects. On the other hand, 3D reconstruction schemes, such as tomosynthesis and CT, require complete knowledge of the X-ray source projection geometry prior to exposure. This limitation precludes much of the potential task-dependent flexibility. This limitation also precludes accurate reconstruction from projections acquired from a patient who moves unpredictably between exposures, as this is geometrically equivalent to not knowing the projection geometry.

Use of digital linear tomosynthesis in imaging of prostheses appears promising. The results of the prosthesis study suggest that digital linear tomosynthesis can improve image quality compared with conventional radiography by removing overlying structures and providing limited 3D information. In addition, the digital linear tomosynthesis method appears to allow for significant improvement of images corrupted by metal artifacts. Digital linear tomosynthesis provided higher quality images than CT. Tomosynthesis is the best solution for cases in which the high-attenuation feature causing the artifacts can be segmented accurately from the projection.

Artifact reduction processing showed an adequate overall performance, but its effectiveness strongly depended on the image region. Digital linear tomosynthesis images gave good results independent of the type of metal present in the patient and showed good results for the removal of noise artifacts, particularly at greater distances from metal objects. The potential for application of digital linear tomosynthesis to the imaging of prostheses appears promising. Flexibility in the choice of imaging parameters in artifact reduction processing based on the desired final images and realistic imaging conditions may be beneficial.

4. Acknowledgment

5. Appendix

5.1 FBP algorithm

The 3D Fourier transform of the 3D volume data generated by the backprojection is based on the following equation (1):

$$F(\omega_x,\omega_y,\omega_z) = \iiint f(x,y,z) \cdot \exp\left\{-j(\omega_x \cdot x + \omega_y \cdot y + \omega_z \cdot z)\right\} dx \cdot dy \cdot dz \tag{1}$$

where $f(x,y,z)$ is the simple backprojection intermediate image, and x, y, and z are real numbers. The meaning of the filtering process performed in 3D Fourier space is described below, and it is mathematically expressed by the following equation (2):

$$FM(\omega_x,\omega_y,\omega_z) = F(\omega_x,\omega_y,\omega_z) \cdot M(\omega_x,\omega_y,\omega_z) \tag{2}$$

where $FM(\omega_x, \omega_y, \omega_z)$ is the filtered 3D Fourier distribution image, and $M(\omega_x, \omega_y, \omega_z)$ is a function representing filter characteristics. The filtering process carried out in 3D Fourier space is to weight the 3D Fourier distribution image of complex data with the real-valued filter function M dependent on the respective frequency values. The weighting function M is compressed in the ω_z direction. $M(\omega_x, \omega_y, \omega_z)$ is expressed by the following equation (3) as a product of three functions representing the filter characteristic:

$$M(\omega_x, \omega_y, \omega_z) = H_{prof}(\omega_z) \cdot H_{spec}(\omega_r) \cdot H_{inverse}(\omega R) \tag{3}$$

$H_{prof}(\omega_z)$ has a low-pass filter characteristic, i.e., a Gaussian characteristic, which is expressed by the following equation (4):

$$H_{prof}(\omega_z) = \exp\left(-0.693\left[\frac{\omega_z}{CFD}\right]^2\right) \tag{4}$$

where CFD is the frequency with the Gaussian attenuation halved.
$H_{spec}(\omega_r)$ has a filter characteristic which is expressed by the following equation (5):

$$\begin{bmatrix} H_{spec}(\omega_r) = 1 & \left(case \quad \omega_r < \frac{CFR - WFR}{2}\right) \\ H_{spec}(\omega_r) = \frac{1 - \sin(\omega_r - CFR) \cdot \pi / WFR}{2} & \left(case \quad \frac{CFR - WFR}{2} < \omega_r < \frac{CFR + WFR}{2}\right). \\ H_{spec}(\omega_r) = 0 & \left(case \quad \frac{CFR + WFR}{2} < \omega_r\right) \end{bmatrix} \tag{5}$$

However, $\omega_r = \sqrt{\omega_x{}^2 + \omega_y{}^2 + \omega_z{}^2}$. The function has a sine wave form with high-frequency components smoothly attenuated. CFR is the cut-off frequency, and WFR is the total transition frequency width of the filter strength. $\frac{CFR + WFR}{2}$ is the Nyquist frequency and $\frac{CFR - WFR}{2}$ is the no-processing region frequency. This $H_{spec}(\omega_r)$ removes high-frequency components from the origin of the 3D Fourier space. $H_{inverse}(\omega R)$ has a filter characteristic which is expressed by the following equation (6):

$$H_{inverse}(\omega R) = |\omega R| \quad , \quad \omega R = \sqrt{\omega_x{}^2 + \omega_y{}^2} \tag{6}$$

The 3D back Fourier transforms the Fourier space data back to 3D volume data, having undergone Fourier space low-pass filtering. The 3D back Fourier transform is expressed by the following equation (7):

$$fm(x, y, z) = \frac{1}{8}\pi^3 \iiint FM(\omega_x, \omega_y, \omega_z) \cdot \exp\left\{j(\omega_x \, x + \omega_y \, y + \omega_z \, z)\right\} d\omega_x d\omega_y d\omega_z \tag{7}$$

where equation (7) is the transformation from the frequency domain to the space domain. It is the inverse of the relation described by equation (1).

5.2 Artifact reduction processing

$H_{inverse}(\omega R)$ has a artifact reduction filter characteristic expressed by the following equation (8):

$$\omega_{R\_temp} = W \ + \ \sqrt{\omega_x^{\ 2} + \omega_y^{\ 2}}$$

$$\omega_{R\_norm} = \frac{\omega_{R\_temp}}{\omega_{R\_max}} \tag{8}$$

$$H_{inverse}(\omega R) = |\omega_{R\_norm}|$$

where W is the addition of a direct current component. ω_{R_max} is the maximum value of a ω_{R_temp} value. The characteristics in the negative direction along the horizontal axis are omitted because these are in linear symmetry about the vertical axis with the characteristics in the positive direction. $H_{spec}(\omega_r) \cdot H_{inverse}(\omega R)$ is expressed by the following equation (9):

$$\begin{cases} H_{spec}(\omega_r) \cdot H_{inverse}(\omega R) = \dfrac{2_{\rho H}}{\pi} \left| |\omega_{R\_norm}| + \sin\left(\dfrac{\pi\rho}{2_{\rho H}} \right) \right| & \left(|\rho| \leq \rho H \right) \\[4mm] H_{spec}(\omega_r) \cdot H_{inverse}(\omega R) = 0 & \left(|\rho| > \rho H \right) \end{cases} \tag{9}$$

ρH is the Nyquist frequency $\left(\dfrac{CFR + WFR}{2} \right)$ and ρ is the no-processing region frequency $\left(\dfrac{CFR - WFR}{2} \right)$.

The 3D back Fourier transforms the Fourier space data back to 3D volume data, having undergone Fourier space low-pass filtering.

6. References

Bleuet P, Guillemaud R, Magin I. Et al. (2002) An adapted fan volume sampling scheme for 3D algebraic reconstruction in linear tomosynthesis. *IEEE transactions on nuclear science*, 49, pp.2366-72, ISSN 0018-9499

Dobbins JT III, Godfrey DJ. (2003) Digital x-ray tomosynthesis: curent state of the art and clinical potential. *Physics in medicine and biology*, 48, R65-106, ISSN 0031-9155

Duryea J, Dobbins JT, Lynch JA. (2003) Digital tomosynthesis of hand joints for arthritis assessment. *Medical Physics*, 30, pp.325-33, ISSN 0094-2405

Feldkamp LA, Davis LC, Kress JW. (1984) Practical cone-beam algorithm. *Journal of the Optical Society of America*, A1, pp.612-619, ISSN 0030-3941

Gomi T, Hirano H, Umeda T. (2009) Evaluation of the X-ray digital linear tomosynthesis reconstruction processing method for metal artifact reduction. *Computerized Medical Imaging and Graphics*, 33, pp.257-274, ISSN 0895-6111

Gomi T, Hirano H. (2008) Clinical potential of digital linear tomosynthesis imaging of total joint arthroplasty. *Journal of Digital Imaging,* 21, pp.312-22, ISSN 0897-1889

Grant DG. Tomosynthesis. (1972) A three-dimensional radiographic imaging technique. *IEEE transactions on bio-medical engineering*, 19, pp.20-8, ISSN 0018-9294

Hsieh J. (1995) computed tomography technology and applications; Image artifacts causes and correction, In: *Medical CT and ultrasound*, LW Goleman, JB Fowlkes, pp.487-518, Advanced Medical Publishing ISBN 1-883526-03-5, Madison

Kak A, Slaney M. (1988) *Principles of computerized tomographic imaging.* IEEE, ISBN 0-89874-494-X, New York

Kamel EM, Burger C, Buck A, et al. (2003) Impact of metallic dental implants on CT-based attenuation correction in a combined PET/CT scanner. *European Radiology*, 13, pp.724-8, ISSN 0938-7994

Man B De, Nuyts J, Dupont P, et al. (2000) Reduction of metal streak artifacts in x-ray computed tomography using a transmission maximum a posteriori algorithm. *IEEE transactions on nuclear science*, 47, pp.997-981, ISSN 0018-9499

Niklason LT, Christian BT, Niklason LE, et al. (1997) Digital tomosynthesis in breast imaging. *Radiology*, 205, pp.399-406, ISSN 0033-8419

Robertson DD, Yuan J, Wang G, et al. (1997) Total hip prosthesis metal-artifact suppression using iterative deblurring reconstruction. *Journal of computer assisted tomography*, 21, pp.293-298, ISSN 0363-8715

Ruttimann U, Groenhuis R, Webber R. (1984) Restoration of digital multilane tomosynthesis by a constrained iteration method. *IEEE transactions on medical imaging*, MI-3, pp.141-8, ISSN 0278-0062

Smith DB. (1985) Image reconstruction from cone-beam projections: necessary and sufficient conditions and reconstruction methods. *IEEE transactions on medical imaging*, M1-4, pp.14-25, ISSN 0278-0062

Sone S, Kasuga T, Sakai F, et al. (1995) Image processing in the digital tomosynthesis for pulmonary imaging. *European Radiology*, 5, pp.96-101, ISSN 0938-7994

Stiel G, Stiel LG, Klotz E et al. (1993) Digital flashing tomosynthesis: A promising technique for angiographic screening. *IEEE transactions on medical imaging*, 12, pp.314-21, ISSN 0278-0062

Wang G, Frei T, Vannier MW. (2000) A fast iterative algorithm for metal artifact reduction in x-ray CT. *Academic Radiology*, 7, pp.607-614, ISSN 1076-6332

Wang G, Snyder DL, O'Sullivan JA, et al. (1996) Iterative debluring for metal artifacts reduction. *IEEE transactions on medical imaging*, 15, pp.657-664, ISSN 0278-0062

Wang G, Vannier MW, Cheng PC. (1999) X-ray cone-beam tomography for metal artifacts reduction and local region reconstruction. *Microscopy and microanalysis*, 5, pp.58-65, ISSN 1431-9276

Wu T, Stewart A, Stanton M, McCauley T, et al. (2003) Tomographic mammography using a limited number of low-dose cone-beam projection images. *Medical Physics*, 30, pp.265-380, ISSN 0094-2405

Ziedses des Plante BG. (1932) Eine neue methode zur differenzierung in der roentgenographie (planigraphie). *Acta radiologica*, 13, pp.182-92, ISSN 0284-1851
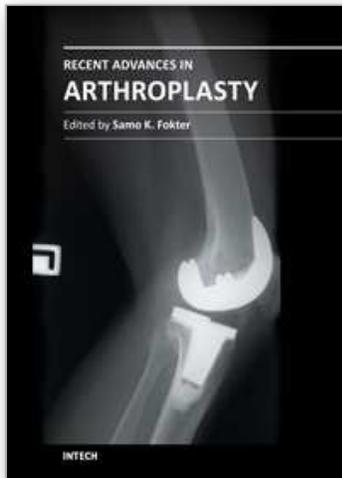
Recent Advances in Arthroplasty

Edited by Dr. Samo Fokter

ISBN 978-953-307-990-5

Hard cover, 614 pages

Publisher InTech

Published online 27, January, 2012

Published in print edition January, 2012

The purpose of this book was to offer an overview of recent insights into the current state of arthroplasty. The tremendous long term success of Sir Charnley's total hip arthroplasty has encouraged many researchers to treat pain, improve function and create solutions for higher quality of life. Indeed and as described in a special chapter of this book, arthroplasty is an emerging field in the joints of upper extremity and spine. However, there are inborn complications in any foreign design brought to the human body. First, in the chapter on infections we endeavor to provide a comprehensive, up-to-date analysis and description of the management of this difficult problem. Second, the immune system is faced with a strange material coming in huge amounts of micro-particles from the tribology code. Therefore, great attention to the problem of aseptic loosening has been addressed in special chapters on loosening and on materials currently available for arthroplasty.

How to reference

In order to correctly reference this scholarly work, feel free to copy and paste the following:

Tsutomu Gomi, Hiroshi Hirano and Masahiro Nakajima (2012). X-Ray Digital Linear Tomosynthesis Imaging of Arthoroplasty, Recent Advances in Arthroplasty, Dr. Samo Fokter (Ed.), ISBN: 978-953-307-990-5, InTech, Available from: http://www.intechopen.com/books/recent-advances-in-arthroplasty/x-ray-digital-linear-tomosynthesis-imaging-of-arthoroplasty

INTECH

open science | open minds